Colloids and Interface Science Communications 9 (2015) 1–5

Contents lists available at ScienceDirect

Colloids and Interface Science Communications

journal homepage: www.elsevier.com/locate/colcom

Theory of Water Desalination by Porous Electrodes with Immobile Chemical Charge

P.M. Biesheuvel [a,b], H.V.M. Hamelers [a], M.E. Suss [c,*]

[a] Wetsus, European Centre of Excellence for Sustainable Water Technology, Leeuwarden, The Netherlands
[b] Laboratory of Physical Chemistry and Soft Matter, Wageningen University, The Netherlands
[c] Faculty of Mechanical Engineering, Technion - Israel Institute of Technology, Haifa, Israel

ARTICLE INFO

Article history:
Received 8 November 2015
Accepted 18 December 2015
Available online 22 February 2016

ABSTRACT

In capacitive deionization (CDI), water is desalinated by storing ions in electrical double layers (EDLs) within the micropores of charged porous carbon electrodes. Recent experiments using chemically modified electrodes have shown differing, novel phenomena such as "inverted CDI," "enhanced CDI," and "inversion peaks." We here present an EDL and dynamic model which includes immobile chemical charge in the micropores and show that the models predict these disparate experimental observations. Our model also makes predictions for a previously undiscovered operational regime with higher salt adsorption, which we term extended voltage CDI.

Capacitive deionization (CDI) is an emerging technology for water desalination which has seen major advances in its theoretical and experimental development over the past decade [1]. In CDI, water is desalinated by the phenomenon of electrosorption in porous carbon electrodes, a capacitive process with significant potential for the desalination of brackish water [1–4]. Upon transferring electronic charge through an external circuit from one porous electrode to the other, electric double layers (EDLs) are formed in the micropores within the carbon electrodes. In micropores, electronic charge (in the carbon) is locally charge-compensated by mobile salt ions, whose transport into and out of the micropores leads to the required difference between cationic and anionic charges to exactly oppose the electronic charge, see Fig. 1 [5–8]. Three charge compensation mechanisms are possible during the electronic charging of the micropores: ion swapping, co-ion repulsion, and counter-ion adsorption [9–11]. Only the latter mechanism, counterion adsorption, results in desalination of the electrolyte outside of the micropores. When counterion adsorption is dominant, more counterions are adsorbed into the micropore EDLs than coions are expelled, and the water flowing through the CDI device is desalinated [1]. When the electrodes become fully charged, the cell can be discharged to release stored ions, resulting in a brine stream. The measurable voltage between the two electrodes is the cell voltage V_{cell} (anode minus cathode potential), and during CDI cell operation, the cell voltage switches between the charging voltage (for instance, $V_{ch} = 1.2$ V), when desalination occurs, to the discharge voltage (typically $V_{disch} = 0$), where brine results.

It has recently been shown experimentally that it is possible for this classical response of a CDI cell to be completely inverted ("inverted-CDI" or i-CDI), or temporarily inverted (so-called "inversion peaks") [12–15]. In i-CDI, during the charging step, salt *desorbs* from the electrodes and the cell effluent is a brine. Ion electrosorption (desalination) occurs only in the cell's discharge step (when $V_{disch} = 0$). This behavior is highly counterintuitive, yet has been leveraged to allow for improved cycle life of CDI cells and has been observed for electrodes modified to contain charged surface groups [13,15,16]. In contrast to fully inverted behavior, a temporary inversion peak has been observed during cell charging when electrodes developed charged oxygenated surfaces during repeated cycling [12–14]. In yet other works, CDI cells with electrodes modified to contain charged surface groups have demonstrated completely different responses, where enhancements in CDI cell salt sorption were observed, but no inversion [17–19]. A quantitative theory which captures and explains these inversion and enhancement phenomena has not yet been proposed. Understanding the causes and implications of these phenomena is of high importance for CDI, as leveraging these effects can lead to significant improvements in CDI cell performance and cycle life.

We here extend classical theory for electrosorption by porous electrodes by including immobile chemical charge in the description of the EDL that forms in the micropores of the electrodes (see Fig. 1) [20]. Thus, our EDL model considers the carbon's electronic charge, the mobile ionic charge in the micropore, and an immobile chemical charge in the micropore. As we show, this extension of classical EDL theory captures the essential features observed in the performance of CDI with chemically modified electrodes, including inverted operation, inversion peaks, and enhanced performance. In addition, our theory demonstrates the existence of a new, unexplored operational mode in which the cell equilibrium salt adsorption capacity (eq-SAC) can be increased significantly compared to what has been previously achieved with capacitive electrodes.

* Corresponding author.
E-mail address: mesuss@technion.ac.il (M.E. Suss).

http://dx.doi.org/10.1016/j.colcom.2015.12.001

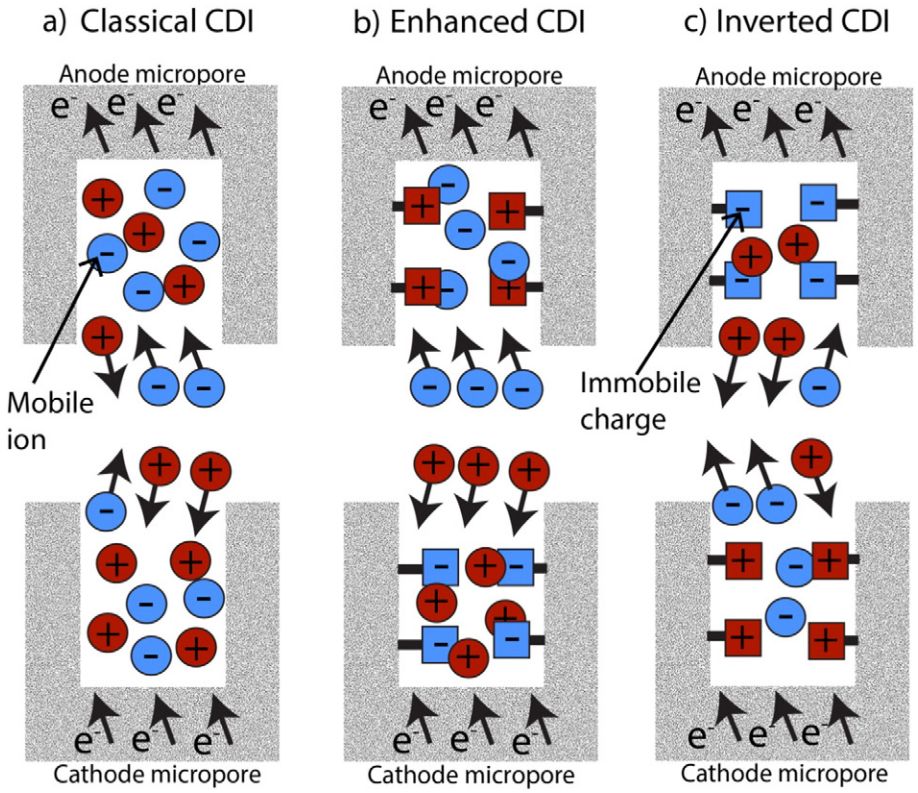

Fig. 1. Diagrams demonstrating mobile ion transport during electronic charging of carbon micropores, where mobile ions are represented as circles and immobile chemical charges as squares. a) For classical CDI with unmodified electrodes, the dominant electronic charge compensation mechanism is counterion adsorption, and the solution outside of the micropore is depleted of ions (desalinated). b, c) For electrodes modified with immobile chemical charge, the charge compensation mechanism and cell performance can be changed drastically. b) For positive immobile charge in the anode and negative in the cathode, parasitic co-ion repulsion is suppressed as the co-ions are immobile, leading to improved desalination (enhanced CDI). c) For negative immobile charges in the anode and positive in the cathode, during charging the dominant mechanism can switch to co-ion repulsion, leading to increased salt concentration outside of the micropores (inverted CDI).

The theory is based on a cell consisting of two porous electrodes separated by an electrolyte-filled spacer channel. The electrolyte is a monovalent salt solution, such as NaCl in water. For classical CDI, the ionic charge density in the micropore EDLs, σ_{ionic}, exactly compensates the electronic charge in the carbon matrix, σ_{elec} (see Fig. 1A). For chemically modified electrodes, we include an immobile chemical charge in the charge balance, and thus $\sigma_{ionic} + \sigma_{chem} + \sigma_{elec} = 0$, taking inspiration from models capturing the semiconductor/water interface [21–25] and porous electrode theory for salinity gradient energy [26,27]. Immobile chemical charges in the micropores in porous carbons will naturally develop by gradual oxidation leading to carboxylic acid groups [12,13] and can be added via the chemical synthesis of sulfonic groups (negative charge) or amine groups (positive charge) [17,28,29], while the basal planes of unmodified carbons adsorb protons and thus will also carry positive charge [30,31].

To describe the EDL structure, we use the Donnan model, which is a simple model that captures the essential physics of salt and charge storage in capacitive porous electrodes [5,6]. Modified versions of the Donnan model accurately describe data for charge and salt adsorption in carbon micropores [1,7,32,33]. The Donnan model is based on the assumption that in carbon micropores (pore size < 2 nm), the EDLs forming along pore surfaces are strongly overlapped. Thus, a single electrostatic potential and concentration in the micropore electrolyte volume can be assumed, and the potential difference between inside and outside the micropore is the Donnan potential, $\Delta\phi_D$. An additional potential drop, $\Delta\phi_S$, is due to a constant capacitance, C_S, between electrolyte volume and carbon matrix which can be due to a Stern layer, or to a quantum capacitance effect [23,34]. In our model formulation, we utilize dimensionless potentials, ϕ, which can be multiplied by the thermal voltage, V_T ($=k_BT/e$) to arrive at voltages, V or E, with units of Volts. At equilibrium, the electrode potential E (potential in the carbon, ϕ_c, relative to the solution phase outside the micropores, ϕ_{ext}) is given by

$$E/V_T = \Delta\phi_S + \Delta\phi_D \tag{1}$$

where potentials $\Delta\phi_S$ and $\Delta\phi_D$ relate to the electronic and ionic charge density according to

$$\Delta\phi_S = \sigma_{elec} \cdot F/C_S \cdot V_T, \quad \Delta\phi_D = -\text{arcsinh}(\sigma_{ionic}/2c_{salt}) \tag{2}$$

where c_{salt} is the salt concentration outside the micropores. Note that all charge densities σ_j are defined per unit micropore volume.

In the Donnan model, the total ion concentration in the micropores, $c_{ions,mi}$, is given by [7]

$$c_{ions,mi}^2 = \sigma_{ionic}^2 + 4 \cdot c_{salt}^2 \tag{3}$$

Eqs. (1)–(3) suffice to calculate the equilibrium ion adsorption in the micropores as a function of electrode potential E, see Fig. S1. To describe a two-electrode CDI cell at equilibrium, we then evaluate Eqs. (1)-(3) for both electrodes, along with

$$V_{cell} = E_A - E_C, \quad m_A \cdot v_{mi,A} \cdot \sigma_{elec,A} + m_C \cdot v_{mi,C} \cdot \sigma_{elec,C} = 0 \tag{4}$$

where m_j is the mass of an electrode (A for anode, C for cathode) and $v_{mi,j}$ is the micropore volume per gram electrode. We analyze the CDI-cycle at two values of V_{cell}, namely, the charging voltage, V_{ch}, and the discharge voltage, V_{disch} (see Fig. 2). By subtracting $c_{ions,mi}$ at the end of charging from $c_{ions,mi}$ at the end of discharging, multiplying by $m_j \cdot v_{mi,j}$, summing over both electrodes, and multiplying by $\frac{1}{2} \cdot M_w/(m_A + m_C)$ ($M_w = 58.44$ g/mol for NaCl), we obtain the

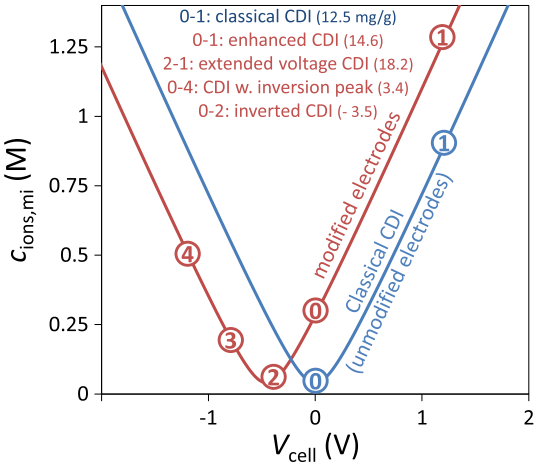

Fig. 2. Model results for total ion concentration in the micropores of a CDI cell, $c_{ions,mi}$, versus cell potential, V_{cell}, for an inflow salt solution, c_{salt}, of 20 mM. The blue curve is the result for classical CDI with unmodified electrodes. The red curve is for a modified cell with immobile chemical charge density of $\sigma_{chem,A} = -\sigma_{chem,C} = 0.4$ M. The presence of chemical charge results in novel operating regimes, where switching between regimes can occur by varying the charging voltage and the discharge voltage. Legend shows the different operating regimes, the numeric representation of the charge and discharge voltages of each regime, and the associated equilibrium salt adsorption capacity in brackets (eq-SAC, in mg/g).

maximum or equilibrium salt adsorption capacity, eq-SAC, expressed in mg salt removal per gram of both electrodes combined [1].

While the above model can be used for two-electrode cells with arbitrary values of the electrode mass, micropore volume, and chemical charge, we now turn our attention to a symmetric two-electrode cell where $m_A = m_C$ $(= m_e)$, $v_{mi,A} = v_{mi,C}$ $(= v_{mi}$, we use $v_{mi} = 0.507$ mL/g) and $\sigma_{chem,A} + \sigma_{chem,C} = 0$ (electrodes contain equal magnitude but opposite sign of the chemical charges). This latter condition results in $c_{ions,mi}$ vs. E curves for the anode and cathode that are mirror-images when reflected in a vertical axis about the point "$E = 0$." Consequently, at equilibrium, the anode potential E_A can be multiplied by a factor of two to obtain the cell voltage, $V_{cell} = 2 \cdot E_A$. For this cell, Eqs. (1)–(4) can be combined in to the simple equation

$$V_{cell} = -2 \cdot V_T \cdot \left(\left(\sigma_{ionic,A} + \sigma_{chem,A} \right) \cdot F / C_S V_T + \operatorname{arcsinh}\left(\sigma_{ionic,A} / 2 c_{salt} \right) \right) \quad (5)$$

which can be used along with Eq. (3) to construct $c_{ions,mi}$ vs. V_{cell} curves. In Fig. 2, we plot such curves, where the blue line shows the predicted curve for an unmodified pair of CDI electrodes ($\sigma_{chem,A} = \sigma_{chem,C} = 0$), and the red line is for our cell of interest ($\sigma_{chem,A} = -\sigma_{chem,C} = 0.4$ M). On the blue curve, "0" denotes discharge at $V_{disch} = 0$, and "1" charging at $V_{ch} = 1.2$ V. The vertical distance between these two points is $\Delta c_{ions,mi} \sim 0.85$ M, which results in an eq-SAC of ~12.5 mg/g. Charging our modified cell from 0 to 1.2 V (from "0" to "1" on the red curve) increases $\Delta c_{ions,mi}$ and eq-SAC to 14.6 mg/g, roughly 20% higher than the unmodified cell. Due to this improved adsorption capacity, we term this operating regime "enhanced CDI" (e-CDI) (see Fig. 1b) [17–19]. Now, if we instead charge the modified cell from state "2" to state "1," where state "2" is at a negative discharge voltage of −0.4 V, we observe an even higher $\Delta c_{ions,mi}$ and eq-SAC of 18.2 mg/g, ~50% higher than the highest eq-SAC obtainable with unmodified electrodes. The latter charging scheme spans 1.6 V and hence we term this operating regime "extended voltage CDI" (eV-CDI). At no point in the cycle for eV-CDI is the cell voltage raised above the thermodynamic potential for water electrolysis (1.23 V). If we now look at a third type of cycle with the modified cell, that from "0" to "3" or from "0" to "2," we see that the micropore ion concentration is lower at the end of the charging step (at "2" or "3") than at the beginning of charging ("0"), or in other words, eq-SAC for the charge process is less than zero. This means that during cell charging, more salt ions are expelled from the micropores than absorbed, a case of inverted CDI (see Fig. 1c) [12,13,15]. As shown in the legend of Fig. 2, this inverted regime is also associated with a strong drop in eq-SAC to 1.2 mg/g ("0" to "3") or 3.5 mg/g ("0" to "2"), where adsorption only occurs during the *discharge* step. Finally, the cycle from "0" to "4", or cycling between 0 V and −1.2 V, demonstrates an eq-SAC of 3.4 mg/g, significantly lower than in a cycle with the exact opposite polarity (cycling between "0" and "1"). While the latter charging process seems unremarkable at the moment, we will show later on that it is associated with temporary inversion peaks during a CDI cycle.

The results of Fig. 2 predict that simply adding immobile chemical charge to micropores can lead to a rich variety of new phenomena, where the charging and discharge voltages play a large role in determining the operational regime (enhanced CDI, inverted CDI, extended voltage CDI, or other). It is important to compare these predictions with experimental data from CDI-cells using chemically charged electrodes. Quantitative comparisons are challenging, as the surface charge magnitude of the electrodes used in the experiments is generally unknown, and the experimental cells' electrodes likely do not possess equal magnitude but opposite sign chemical charge. However, various qualitative comparisons can be made. For example, Gao *et al.* utilized cells with an anode with negative chemical charge and a cathode with positive chemical charge, and observed an inverted CDI response for $V_{ch} = 0.8$ and 1.1 V [15,29]. Our model also predicts inversion for a cell with an anode with negative chemical charge and a cathode with positive chemical charge (for example, charging from "0" to "2" or "3" in Fig. 2, see also Fig. 1c). Further, Gao *et al.* report the peculiar phenomenon that eq-SAC decreases with increasing charging voltage, for example, when going from charging at 0.8 V to –0.9 V [15]. Our model predicts the same behavior, for example, charging from 0 to −0.4 V ("0" to "2," Fig. 2) with modified electrodes gives higher eq-SAC than charging from 0 to −0.8 V ("0" to "3"). As a second point of comparison, we look at the paper of Cohen *et al.* [13], where decreasing cell performance was attributed to the increasingly negative chemical charge of the anode as it oxidized upon repeated cell cycling, and further performance was recovered reversing cell polarity. In our model, we observe a similar effect where SAC decreases significantly when the anode is modified with a negative chemical charge (from "0" to "4," see Fig. 2), yet eq-SAC improves dramatically when polarity is reversed (from "0" to "1" on the red curve). As another point of comparison, Yang *et al.* observed a ~20% enhancement in CDI cell salt storage upon functionalizing the surface of carbon nanotube anodes with positive charge [17]. Wu *et al.* observed a ~50% improvement in salt adsorption with a modified cathode with negative chemical charges via adding carboxylic groups to the carbon surface [19]. The latter two observations of "enhanced CDI" occur when the chemical charge is of the same sign as the electrode's co-ion (see Fig. 1). Our model predicts "enhanced CDI" (an enhanced value of eq-SAC) for the case of positive chemical charge in the anode and negative in the cathode, which is roughly 20% for 0–1.2 V charging ("0" to "1" on the red curve compared to "0" to "1" on the blue curve of Fig. 2). For the case of enhanced voltage CDI (eV-CDI), there is no experimental data using chemically charged electrodes to demonstrate this regime. Capacitive electrodes have until now been able to attain roughly 14 mg/g eq-SAC [1], and eV-CDI promises significant enhancements to this value (our model predicts >18 mg/g). Note the improvement in eq-SAC predicted in Fig. 2 is obtained with a chemical charge density of ±0.4 M. Commercial ion-exchange membranes have immobile charge densities in excess of 5 M per unit aqueous pore volume in the membrane [35] and thus higher values than 0.4 M may be experimentally feasible in porous carbons, boosting further eq-SAC.

We now introduce a simple dynamic model for desalination in a CDI cell including immobile chemical charge, in order to further study the operational regimes and gain insight into the underlying mechanism. Our simple dynamic model of a CDI cell assumes no internal mass transfer limitations in the electrodes and assumes that ionic current is

proportional to an Ohmic potential drop, $\Delta\phi_\Omega$, across the spacer channel. More detailed theories for porous electrodes and spacers (including ion concentration variations) are given in refs. [1,2,4,32,36–41]. The electronic current I running through the external circuit from cathode to anode equals the ionic current running through the electrolyte in opposite direction. For electrodes without Faradaic reactions, a balance for the electronic charge in each electrode is given by

$$m_j \cdot \nu_{mi,j} \cdot \frac{\partial \sigma_{elec,j}}{\partial t} = \pm I/F \tag{6}$$

where "+" is used for j = A and "−" for j = C. The ionic current relates to an Ohmic potential drop according to

$$I = \Delta V_\Omega / R_\Omega. \tag{7}$$

In the transport model, ΔV_Ω is added to the right-hand side of Eq. (4a). In Eq. (7), R_Ω is an Ohmic transport resistance (dimension of Ω) which we assume is inversely proportional to the salt concentration, c_{salt}, according to $R_\Omega = \alpha/c_{salt}$.

Desalination of the water in the CDI cell is described by the salt balance

$$V_{tot} \cdot \frac{\partial c_{salt}}{\partial t} = \Phi \cdot (c_{salt,in} - c_{salt,out}) - \frac{1}{2} \cdot (J_{ions,A} + J_{ions,C}), \tag{8}$$

where V_{tot} is the electrolyte volume in the cell excluding micropores, Φ the solution flowrate through the cell, $c_{salt,in}$ and $c_{salt,out}$ salt concentrations in the inflow and outflow (effluent) of the cell, and $J_{ions,j}$ the ion flow rates from spacer to electrode micropores (in units of mol/s). In this "stirred tank" mass balance, Eq. (8), c_{salt} is the salt concentration everywhere in the cell (except micropores), and thus also the salt concentration of the effluent ($c_{salt,out} = c_{salt}$). Finally, the ion flow rate into each electrode is given by.

$$m_j \cdot \nu_{mi,j} \cdot \frac{\partial c_{ions,mi,j}}{\partial t} = J_{ions,j}. \tag{9}$$

This set of differential algebraic equations suffices for a first-order model to simulate a CDI process that has immobile chemical charges in one or both electrodes. Calculation results are based on a symmetric cell, C_S = 170 F/mL, $V_{tot}/(m_e \cdot \nu_{mi}) = \beta = 10$ (lower two curves in Fig. 3a) or $\beta = 15$ (upper three curves in Fig. 3a), residence time $V_{tot}/\Phi = 16$ s, and a transport resistance $\alpha \cdot m_e \cdot \nu_{mi} = 1\ \mu\Omega \cdot$mol. Calculations in Fig. 3b assume for the spacer channel $c_{salt,out} = c_{salt,in}$ and thus the results do not depend on β. In Fig. 3a, we plot the results of the dynamic model in the form of $c_{salt,effluent}$ versus t for the same chemical charge density and voltage ranges (and thus the same eq-SAC) as the cases tabulated in Fig. 2. Here we simulated a charge–discharge cycle where for the first 100 s, the cell undergoes a charging step, and for the following 100 s, the cell is discharged. Our model results show similar characteristics as experimental data from CDI cells with chemically charged electrodes [12–15], such as an inversion peak (red curve) and inverted CDI operation (blue curve), and neither of these dynamical features is captured by previous CDI theory [1,32,36,39]. The differences in dynamics between classical CDI (green curve), e-CDI (purple curve), and eV-CDI (yellow curve) are subtle, but significant differences exist in equilibrium salt adsorption capacity (see value of eq-SAC listed along each curve in Fig. 3a and in Fig. 2). In Fig. 3b, we again plot the results of our dynamic model, but now in the form of counterion flux into the micropores, $J_{counter}$, divided by co-ion flux out of the micropores, $-J_{co}$, versus time during charging. This parameter, $\gamma = -J_{counter}/J_{co}$, provides insight into the charge compensation mechanism, as when it is greater than unity, the dominant charge compensation mechanism is counterion adsorption, and if less than unity, we instead have primarily co-ion expulsion. When the parameter equals unity (thin dashed line in Fig. 3b), we have ion swapping as the sole charge compensation mechanism. As can be seen, classical CDI with unmodified electrodes (green curve) behaves as expected, beginning with ion swapping at early times (small voltages), and progressing to significant counterion adsorption at later times (large voltages) [36]. Including immobile chemical charge has a drastic effect on the charge compensation mechanism. For e-CDI (purple curve) and eV-CDI (yellow curve), the dominant mechanism is counterion adsorption but with a higher ratio of counterion to coion flux than classical CDI. Thus, the latter two regimes enable higher salt storage and reduced parasitic energy losses due to co-ion current. For CDI with inversion peaks (red curve), the dominant mechanism switches over time from initially co-ion repulsion, which coincides with when the inversion peak is seen in Fig. 3a, to counterion

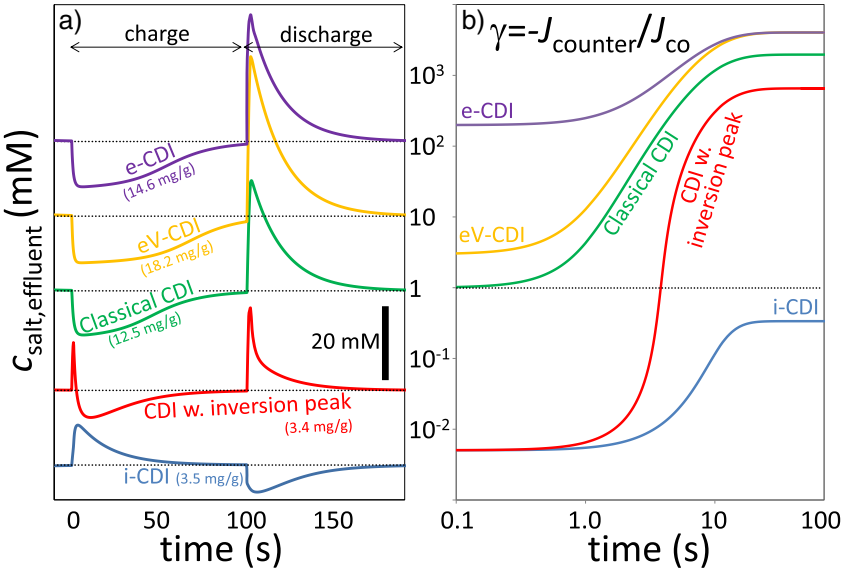

Fig. 3. Results of our dynamic model capturing CDI desalination dynamics. a) Effluent salt concentration, for charging from 0 to 100 s and discharging from 100 to 200 s. For each regime (see curve labels), the cell charging and discharge voltage, chemical charge density, $c_{salt,in}$, and eq-SAC value (included in the label for each curve) are the same as in Fig. 2. The model reproduces key features observed in experiments, including inversion peaks and inverted behavior. b) The ratio, γ, of counterion flux, $J_{counter}$, over co-ion flux, $-J_{co}$, into the micropores during cell charging, where a ratio above unity indicates that counterion adsorption is the dominant mechanism for charge compensation. The presence of immobile charge drastically affects the charge compensation when compared to classical CDI.

adsorption. For i-CDI, the dominant mechanism remains always co-ion repulsion, consistent with the fully inverted dynamics seen in Fig. 3a. The current efficiency λ has been defined [1] as the ratio of total ion flux over current, thus $\lambda = (J_{counter} + J_{co})/(J_{counter} - J_{co})$. As we defined the y-axis of Fig 3b as $\gamma = -J_{counter}/J_{co}$, we can relate γ and λ according to $\lambda = (\gamma - 1)/(\gamma + 1)$. Thus, we can see that adding chemical charge significantly modifies a CDI cell's current efficiency. For example, the enhanced CDI regime has $\lambda \sim 1$ for the entire charging step, unlike classical CDI which only approaches $\lambda \sim 1$ at later times (here after several seconds). Conversely, for i-CDI, we see that $\gamma < 1$ and $\lambda < 0$ for the entire charging process, i.e., the current efficiency remains negative. As current efficiency has a big effect on the energy use the desalination process [1], we conclude that chemical charge present in porous electrodes not only influences the desalination performance, but also the energy efficiency of the CDI process.

In conclusion, we present novel EDL and dynamic models which include immobile chemical charge in the carbon micropores. These models capture and explain the wide variety of experimental observations related to CDI cells with chemically charged electrodes, including inverted CDI, inversion peaks, and enhanced CDI. We further show the existence of a new operational regime of "extended voltage CDI" where for suitably chemically modified electrodes extending the voltage range improves salt adsorption by ~50% over typical CDI electrodes. Overall, we believe our model establishes a theoretical foundation for the promising field of CDI with chemically charged porous electrodes.

Acknowledgments

This work was performed in the cooperation framework of Wetsus, European Centre of Excellence for Sustainable Water Technology (www.wetsus.eu). Wetsus is co-funded by the Dutch Ministry of Economic Affairs and Ministry of Infrastructure and Environment, the Province of Fryslân, and the Northern Netherlands Provinces. We thank Xin Gao, James Landon, and Ayokunle Omosebi (University of Kentucky, USA) for useful suggestions during preparation of this manuscript.

Appendix A. Supplementary Data

Supplementary data to this article can be found online at http://dx.doi.org/10.1016/j.colcom.2015.12.001.

References

[1] M.E. Suss, S. Porada, X. Sun, P.M. Biesheuvel, J. Yoon, V. Presser, Energy Environ. Sci. 8 (2015) 2296.
[2] A.M. Johnson, J. Newman, J. Electrochem. Soc. 118 (1971) 510.
[3] R.A. Rica, R. Ziano, D. Salerno, F. Mantegazza, D. Brogioli, Phys. Rev. Lett. 109 (2012) 156103.
[4] M. Mirzadeh, F. Gibou, T.M. Squires, Phys. Rev. Lett. 113 (2014) 097701.
[5] M. Müller, B. Kastening, J. Electroanal. Chem. 374 (1994) 149.
[6] B. Kastening, M. Heins, Electrochim. Acta 50 (2005) 2487.
[7] P.M. Biesheuvel, S. Porada, M. Levi, M.Z. Bazant, J. Solid State Electrochem. 18 (2014) 1365.
[8] B. Giera, N.J. Henson, E.M. Kober, M.S. Shell, T.M. Squires, Langmuir 31 (2015) 3553.
[9] M.D. Levi, G. Salitra, N. Levy, D. Aurbach, J. Maier, Nat. Mater. 8 (2009) 872.
[10] C. Prehal, D. Weingarth, E. Perre, R.T. Lechner, H. Amenitsch, O. Paris, V. Presser, Energy Environ. Sci. 8 (2015) 1725.
[11] J.M. Griffin, A.C. Forse, W.-Y. Tsai, P.-L. Taberna, P. Simon, C.P. Grey, Nat. Mater. 14 (2015) 812.
[12] Y. Bouhadana, E. Avraham, M. Noked, M. Ben-Tzion, A. Soffer, D. Aurbach, J. Phys. Chem. C 115 (2011) 16567.
[13] I. Cohen, E. Avraham, Y. Bouhadana, A. Soffer, D. Aurbach, Electrochim. Acta 153 (2015) 106.
[14] X. Gao, A. Omosebi, J. Landon, K. Liu, J. Electrochem. Soc. 161 (2014) E159.
[15] X. Gao, A. Omosebi, J. Landon, K. Liu, Energy Environ. Sci. 8 (2015) 897.
[16] A. Omosebi, X. Gao, J. Rentschler, J. Landon, K. Liu, J. Colloid Interface Sci. 446 (2015) 345.
[17] J. Yang, L. Zou, N.R. Choudhury, Electrochim. Acta 91 (2013) 11.
[18] M. Andelman, J. Mater. Sci. Chem. Eng. 2 (2014) 16.
[19] T. Wu, G. Wang, Q. Dong, B. Qian, Y. Meng, J. Qiu, Electrochim. Acta 176 (2015) 426.
[20] P.M. Biesheuvel, M.E. Suss, H.V.M. Hamelers, Arxiv (2015) 1506.03948.
[21] H. Gerischer, P. Delahay, Adv. Electrochem. Electrochem. Eng. 1 (1961) 139 Interscience.
[22] R. Memming, G. Schwandt, Angew. Chem. Int. Ed. 6 (1967) 851.
[23] H. Gerischer, R. McIntyre, D. Scherson, W. Storck, J. Phys. Chem. 91 (1987) 1930.
[24] Z. Jiang, D. Stein, Phys. Rev. E 83 (2011) 031203.
[25] M.E. Fleharty, F. van Swol, D.N. Petsev, Phys. Rev. Lett. 113 (2014) 158302.
[26] D. Brogioli, R. Ziano, R.A. Rica, D. Salerno, F. Mantegazza, J. Colloid Interface Sci. 407 (2013) 457.
[27] M.M. Fernández, et al., J. Power Sources 302 (2016) 387.
[28] M. Marino, et al., J. Colloid Interface Sci. 436 (2014) 146.
[29] X. Gao, A. Omosebi, J. Landon, K. Liu, Environ. Sci. Technol. 49 (2015) 10920.
[30] M.A. Montes-Morán, D. Suárez, J.A. Menéndez, E. Fuente, Carbon 42 (2004) 1219.
[31] H.P. Boehm, Carbon 32 (1994) 759.
[32] T. Kim, J.E. Dykstra, S. Porada, A. van der Wal, J. Yoon, P.M. Biesheuvel, J. Colloid Interface Sci. 446 (2015) 317.
[33] P.M. Biesheuvel, Arxiv (2015) 1509.06354.
[34] L.-H. Shao, et al., PCCP 12 (2010) 7580.
[35] A.H. Galama, J.W. Post, M.A. Cohen Stuart, P.M. Biesheuvel, J. Membrane Sci. 442 (2013) 131.
[36] P.M. Biesheuvel, M.Z. Bazant, Phys. Rev. E 81 (2010) 031502.
[37] R.A. Rica, R. Ziano, D. Salerno, F. Mantegazza, M.Z. Bazant, D. Brogioli, Electrochim. Acta 92 (2013) 304.
[38] M.E. Suss, P.M. Biesheuvel, T.F. Baumann, M. Stadermann, J.G. Santiago, Environ. Sci. Technol. 48 (2014) 2008.
[39] J. Gabitto, C. Tsouris, Transp. Porous Media 109 (2015) 61.
[40] A. Hemmatifar, M. Stadermann, J.G. Santiago, J. Phys. Chem. C 119 (2015) 24681.
[41] J.E. Dykstra, R. Zhao, P.M. Biesheuvel, A. van der Wal, Water Res. 88 (2016) 358.